# Self-induced stimulated light scattering in nematic liquid crystals: Theory and experiment

L. Marrucci, G. Abbate, S. Ferraiuolo, P. Maddalena, and E. Santamato
*Dipartimento di Scienze Fisiche, Università Federico II, Mostra d'Oltremare, Padiglione 20, I-80125 Napoli, Italy*
(Received 21 April 1992)

We present a theoretical and experimental study of the molecular collective rotation induced in a nematic liquid crystal by a laser beam, when self-induced stimulated light scattering takes place. The model is accurate enough to obtain quantitative agreement with experimental results, including the observation of optical bistability and hysteresis. Exact plane-wave expressions for energy and angular-momentum exchange between light and matter are also derived.

PACS number(s): 61.30.Gd, 42.65.−k, 64.70.Md

## I. INTRODUCTION

A phenomenon of nonlinear optics called self-induced stimulated light scattering (SISLS) has been recently observed [1] in a thin film of nematic liquid crystal (NLC), prepared in the homeotropic alignment.

To observe this phenomenon a circularly polarized laser beam must be focused on the sample at normal incidence. When the light intensity $I$ is raised above a threshold value, the emerging light becomes elliptically polarized, with the ellipse major axis rotating at constant speed (a more general SISLS where the input light is already elliptically polarized has also been studied in Ref. [2]).

This interesting nonstationary effect can be understood in terms of direct angular-momentum exchange between the light beam and the collective orientational degrees of freedom of the medium. In a quantum picture, the process is described as a photon stimulated scattering: each scattered photon goes from the initial helicity state to a final state with opposite helicity, thus imparting to the medium an angular momentum of $2\hbar$, directed along the propagation direction $\hat{\mathbf{z}}$. If $p$ photons are scattered per unit time, the angular-momentum transfer produces a constant torque, $\tau_z = 2\hbar p$, acting on the medium, which induces a rotation of the average molecular orientation (i.e., of the director $\hat{\mathbf{n}}$) around $\hat{\mathbf{z}}$. At steady state, this torque is balanced by the viscous torque, and the angular velocity $\Omega$ of the molecular rotation is constant in time.

During this process, energy is continuously dissipated by viscous forces in the medium; this energy is supplied by the light itself. The medium being transparent, the photons cannot be absorbed. Consequently, each photon reversing its helicity must suffer a frequency redshift $\Delta\omega$, so that its energy is lowered by an amount $\hbar\Delta\omega$. The predicted redshift has been experimentally measured [3]. The frequency difference between the two helicity components of the emerging light also appears in the rotation of the polarization ellipse.

The relationship between the redshift $\Delta\omega$ and the angular velocity $\Omega$ can be obtained in a very simple way: the work per unit time done by the optical torque $\tau_z$ on $\hat{\mathbf{n}}$ is $\tau_z\Omega = 2\hbar p\Omega$; this work is to be equated to the energy lost by photons per unit time $\hbar\Delta\omega p$, thus obtaining $\Delta\omega = 2\Omega$. Since in the final relation $\hbar$ disappeared, such a relationship is expected to be found also on purely classical grounds (as in fact will be shown in Sec. IV).

SISLS can be looked upon as a kind of stimulated Brillouin light scattering, where collective orientational modes are involved. Nevertheless, due to the very large viscosity acting on these modes, no free oscillation is possible in the medium, contrary to Brillouin scattering. This implies the following peculiarities of SISLS: (i) there is no anti-Stokes production; (ii) the frequency shift amplitude $2\Omega$ is much smaller than usual Brillouin shifts (typical values of $\Omega$ are $10^{-1}$–$10^{-2}$ Hz); (iii) the frequency $\Omega$ is not determined by the medium, but varies with the intensity $I$ of the laser beam itself; (iv) the light intensity necessary to observe the phenomenon is very small and commercial continuous-wave lasers can be used.

Both experiment [4,5] and theory [6,7] show that, for homeotropic samples where the director $\hat{\mathbf{n}}$ is perpendicular to the bounding walls, there exists a threshold value $I_{\rm th}$ for the light intensity below which the molecular reorientation cannot be induced. This threshold effect is called the optical Fréedericksz transition (OFT), and it has been studied extensively with linearly polarized light where SISLS does not occur.

A peculiar feature of SISLS is that the transition to the rotating regime is first order. This is somewhat unexpected, since all known OFT's are second order [8]. As usual with first-order transitions, hysteresis is also observed. Indeed, even if the intensity $I$ is lowered below $I_{\rm th}$, the rotation regime remains stable as long as $I$ is above a second critical value $I_1 < I_{\rm th}$. Below this second threshold value the rotation ceases, and the director $\hat{\mathbf{n}}$ relaxes to the initial homeotropic alignment.

All known models of OFT in nematic liquid crystals assume either splay-bend or twist reorientation separately [7]. Theoretical studies of SISLS were recently carried out in the case where the molecular director $\hat{\mathbf{n}}$ is uniformly tilted out of the $z$ axis at a fixed angle (as in smetic-$C$ liquid crystals) [9], and in the case where twist distortion is absent [10]. In all these models the orientational degrees of freedom are reduced to a single one, thus greatly simplifying the problem. Relevant features observed in SISLS (such as the occurrence of first-order OFT) remain yet unexplained, however.

 

Although including both degrees of freedom of $\hat{\mathbf{n}}$ greatly increases the complexity of the problem, analytical results can be obtained, which agree even quantitatively with the observed phenomena. In the present work, such a theoretical analysis of SISLS is presented and compared with experiments.

The paper is organized as follows. First, in the classical framework of continuum physics, the general field equations of the model are derived in Sec. II, and the main approximations are explicitly stated. The time dependence of the asymptotic rotating regimes is found in Sec. III, where the equations for the field spatial dependence are also obtained. In Sec. IV, the results of the preceding section are used to evaluate the angular-momentum and energy transfer from light to matter, and the connection with the quantum picture is established. In Sec. V, an approximate analytic solution of the spatial equations is presented, which is found to be sufficiently accurate to explain most of the observed phenomena. Finally, in Sec. VI the experimental results are reported and quantitatively compared with theory.

## II. DYNAMICAL EQUATIONS

The macroscopic local properties of a nematic liquid crystal are described by a unit vector field $\hat{\mathbf{n}}$ which indicates the average molecular orientation [11,12]. The hydrodynamical degrees of freedom (velocity field), although coupled with $\hat{\mathbf{n}}$, will be neglected for simplicity (we are thus neglecting the "back-flow" effect [13,14]). Also, the temperature and density (or pressure) fields, supposed to be uniform and fixed, will not enter the problem (apart from the obvious dependencies of the phenomenological constants).

Let us consider an infinite layer of NLC of thickness $L$. We use the Cartesian coordinate system indicated in Fig. 1, as well as polar angles $\vartheta$ and $\varphi$ to specify $\hat{\mathbf{n}}$, where $\vartheta$ is the tilt angle between $\hat{\mathbf{n}}$ and the $z$ axis, and $\varphi$ is the azimuthal angle between the $\hat{\mathbf{n}}z$ plane and the $xz$ plane. The laser wave is described by the complex electric amplitude $\mathbf{E}$, whose real part is the actual electric field of the wave. Both $\hat{\mathbf{n}}$ and $\mathbf{E}$ depend continuously on the point $(x,y,z)$ and on time $t$.

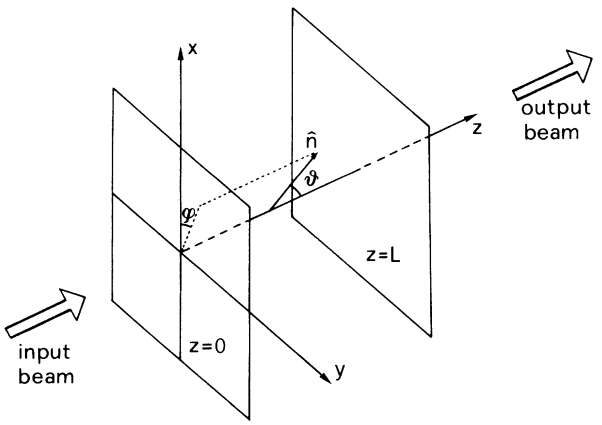


FIG. 1. The NLC layer, with the Cartesian coordinate system and the polar angles $\vartheta$ and $\varphi$ for the molecular director $\hat{\mathbf{n}}$.

We assume that the impinging light beam is a monochromatic plane wave, of frequency $\omega/2\pi$, traveling in the positive $z$-axis direction, and entering the sample at $z=0$. Let $c$ and $\lambda=2\pi c/\omega$ be the velocity of light and wavelength in vacuum, respectively, and $I$ the input beam intensity, as given by the $z$ component of the Poynting vector averaged over a cycle.

Because the geometry is symmetric to translations in the $xy$ plane, we can suppose that all fields inherit this symmetry. We assume therefore that the only relevant spatial coordinate is $z$ (plane symmetry approximation).

The electric displacement vector $\mathbf{D}$ is linked to $\mathbf{E}$ through the dielectric tensor $\epsilon$:

$$D_i=\epsilon_{ij}E_j \quad (i,j=x,y,z) \tag{1}$$

(sum over repeated indices is implied), with

$$\epsilon_{ij}=\epsilon_\perp\delta_{ij}+\epsilon_a n_i n_j \ . \tag{2}$$

Here $\epsilon_\perp=n_o^2$ is the square of the ordinary refractive index of the NLC, and $\epsilon_a=\epsilon_\parallel-\epsilon_\perp$, where $\epsilon_\parallel=n_e^2$ is the square of the extraordinary refractive index. The medium is assumed nonmagnetic and nonabsorbing ($\epsilon$ is real).

In our plane geometry, Maxwell's equation

$$\mathrm{div}\mathbf{D}=0 \tag{3}$$

allows one to eliminate $E_z$ from the set of independent fields. Maxwell's equations for the remaining transverse amplitudes $E_x$ and $E_y$ are then written as

$$\frac{\partial^2 E_i}{\partial z^2}-\frac{1}{c^2}\frac{\partial^2}{\partial t^2}\bar{\epsilon}_{ij}E_j=0 \quad (i,j=x,y) \ , \tag{4}$$

where

$$\bar{\epsilon}_{ij}=\left[\epsilon_{ij}-\frac{\epsilon_{iz}\epsilon_{zj}}{\epsilon_{zz}}\right] \quad (i,j=x,y) \ . \tag{5}$$

Equation (4) can be rewritten in terms of the right $E_R$ and left $E_L$ circular polarization amplitudes of $\mathbf{E}$, connected to the Cartesian amplitudes by the transformation rules

$$\begin{bmatrix}E_R\\E_L\end{bmatrix}=\frac{1}{\sqrt{2}}\begin{bmatrix}1 & i\\1 & -i\end{bmatrix}\begin{bmatrix}E_x\\E_y\end{bmatrix} \ . \tag{6}$$

Explicitly, we find

$$\begin{aligned}&\frac{\partial^2 E_R}{\partial z^2}-\frac{1}{c^2}\frac{\partial^2}{\partial t^2}\left[\frac{\bar{n}^2+n_o^2}{2}E_R+\frac{\epsilon_a\bar{n}^2}{2\epsilon_\parallel}Q^2E_L\right]=0 \ ,\\ &\frac{\partial^2 E_L}{\partial z^2}-\frac{1}{c^2}\frac{\partial^2}{\partial t^2}\left[\frac{\bar{n}^2+n_o^2}{2}E_L+\frac{\epsilon_a\bar{n}^2}{2\epsilon_\parallel}Q^{*2}E_R\right]=0 \ ,\end{aligned} \tag{7}$$

where the complex field $Q$ is given by

$$Q=\sin\vartheta e^{i\varphi} \tag{8}$$

and the asterisk denotes complex conjugation. The effective index $\bar{n}(\vartheta)$ appearing in Eqs. (7) is given by

$$\bar{n}(\vartheta)=\frac{n_o n_e}{(n_o^2\sin^2\vartheta+n_e^2\cos^2\vartheta)^{1/2}} . \tag{9}$$

Equations (7) must be coupled with the equation for $Q$, or equivalently for the two real fields $\vartheta$ and $\varphi$, describing the local orientation of the director $\hat{\mathbf{n}}$. The last equation is obtained by balancing the elastic, electromagnetic, and viscous torques acting on $\hat{\mathbf{n}}$ (see Ref. [11]):

$$\tau_d+\tau_{\rm em}+\tau_v=\mathbf{0} . \tag{10}$$

The elastic and electromagnetic torques $\tau_d$ and $\tau_{\rm em}$ can be found as the (functional) derivative of the total free energy with respect to a local variation of $\hat{\mathbf{n}}$, while the viscous torque $\tau_v$ is obtained as the derivative of the system dissipation function with respect to a variation of $\dot{\mathbf{n}}=\partial\hat{\mathbf{n}}/\partial t$.

The free-energy density of $F$ of a NLC in an external electromagnetic field (as a potential of $\hat{\mathbf{n}}$, $\mathbf{E}$, and $\mathbf{H}$) is the sum of elastic and electromagnetic contributions:

$$F=F_d+F_{\rm em} . \tag{11}$$

The term $F_d$ is the classical Frank elasticity energy, given by [11]

$$F_d=\tfrac{1}{2}K_{11}(\,\mathrm{div}\hat{\mathbf{n}})^2+\tfrac{1}{2}K_{22}(\hat{\mathbf{n}}\cdot\,\mathrm{rot}\hat{\mathbf{n}})^2+\tfrac{1}{2}K_{33}(\hat{\mathbf{n}}\times\,\mathrm{rot}\hat{\mathbf{n}})^2 , \tag{12}$$

where $K_{11}$, $K_{22}$, and $K_{33}$ are the splay, twist, and bend elastic constants, respectively. In our geometry, Eq. (12) becomes ($\partial/\partial z$ is denoted with a prime)

$$F_d=\frac{K_{33}}{2}[(1-p_1\sin^2\vartheta)\vartheta'^2+(1-p_2\sin^2\vartheta)\sin^2\vartheta\varphi'^2] , \tag{13}$$

with

$$\begin{aligned} p_1&=1-K_{11}/K_{33} ,\\ p_2&=1-K_{22}/K_{33} . \end{aligned} \tag{14}$$

The nonzero components of $\tau_d$ are obtained from $F_d$ as

$$\begin{aligned} \tau_{d,\vartheta}&=\frac{\partial}{\partial z}\frac{\partial F_d}{\partial\vartheta'}-\frac{\partial F_d}{\partial\vartheta}\\ &=K_{33}[(1-p_1\sin^2\vartheta)\vartheta''-\frac{p_1}{2}\sin2\vartheta\vartheta'^2\\ &\quad-(\tfrac{1}{2}-p_2\sin^2\vartheta)\sin2\vartheta\varphi'^2] .\\ \tau_{d,\varphi}&=\frac{\partial}{\partial z}\frac{\partial F_d}{\partial\varphi'}-\frac{\partial F_d}{\partial\varphi}=\frac{\partial}{\partial z}[K_{33}(1-p^2\sin^2\vartheta)\sin^2\vartheta\varphi'] . \end{aligned} \tag{15}$$

The term $F_{\rm em}$ is the usual electromagnetic (cycle-averaged) free-energy density in a linear (at fixed $\hat{\mathbf{n}}$) dielectric and is given by [15]

$$\begin{aligned} F_{\rm em}&=\frac{\mathbf{D}\cdot\mathbf{E}^*+\mathbf{H}\cdot\mathbf{H}^*}{16\pi}\\ &=-\frac{\epsilon_a}{16\pi}(\hat{\mathbf{n}}\cdot\mathbf{E})(\hat{\mathbf{n}}\cdot\mathbf{E}^*)-\frac{\epsilon_\perp\mathbf{E}\mathbf{E}^*+\mathbf{H}\mathbf{H}^*}{16\pi} . \end{aligned} \tag{16}$$

As before, $F_{\rm em}$ can be used to find the electromagnetic torque $\tau_{\rm em}$ acting on $\hat{\mathbf{n}}$:

$$\begin{aligned} \tau_{{\rm em},\vartheta}&=\frac{\partial}{\partial z}\frac{\partial F_{\rm em}}{\partial\vartheta'}-\frac{\partial F_{\rm em}}{\partial\vartheta}\\ &=\frac{\epsilon_a\bar{n}^4\sin\vartheta\cos\vartheta}{16\pi\epsilon_\perp\epsilon_\parallel}\\ &\quad\times\left[|E_R|^2+|E_L|^2+\frac{2}{|Q|^2}\,\mathrm{Re}(E_R^*E_LQ^2)\right] ,\\ \tau_{{\rm em},\varphi}&=\frac{\partial}{\partial z}\frac{\partial F_{\rm em}}{\partial\varphi'}-\frac{\partial F_{\rm em}}{\partial\varphi'}=-\frac{\epsilon_a\bar{n}^2}{8\pi\epsilon_\parallel}\,\mathrm{Im}(E_R^*E_LQ^2) . \end{aligned} \tag{17}$$

In deriving Eqs. (17), we used Eq. (3) to eliminate $E_z$ (Re and Im denote the real and imaginary part of the argument, respectively).

The dissipation function density in the absence of velocity field is taken as

$$R=\tfrac{1}{2}\gamma_1(\dot{\mathbf{n}})^2 , \tag{18}$$

where $\gamma_1$ is the orientational viscosity [11]. Therefore we get

$$\begin{aligned} \tau_{v,\vartheta}&=-\frac{\partial R}{\partial\dot{\vartheta}}=-\gamma_1\dot{\vartheta} ,\\ \tau_{v,\varphi}&=-\frac{\partial R}{\partial\dot{\varphi}}=-\gamma_1\sin^2\vartheta\dot{\varphi} . \end{aligned} \tag{19}$$

The torque balance Eq. (10) is finally written out in the evolution form:

$$\begin{aligned} \dot{\vartheta}&=\frac{1}{\gamma_1}[\tau_{d,\vartheta}(\vartheta'',\vartheta',\varphi',\vartheta)+\tau_{{\rm em},\vartheta}(\vartheta,\varphi,E_R,E_L)] ,\\ \dot{\varphi}&=\frac{1}{\gamma_1\sin^2\vartheta}[\tau_{d,\varphi}(\varphi'',\vartheta',\varphi',\vartheta)+\tau_{{\rm em},\varphi}(\vartheta,\varphi,E_R,E_L)] , \end{aligned} \tag{20}$$

where the torque expressions are given by Eqs. (15) and (17).

The nonlinear set of Eqs. (7) and (20), when completed with the appropriate boundary conditions, describes the dynamics of our system. We must specify $E_R$ and $E_L$ (or $E_x$ and $E_y$) entering the sample. We also assume that $\hat{\mathbf{n}}$ is normal to the bounding surfaces at all times (strong homeotropic anchoring), i.e.,

$$n_x(0)=n_y(0)=n_x(L)=n_y(L)=0 . \tag{21}$$

Although Eqs. (21) express four independent boundary conditions on $\hat{\mathbf{n}}$, these reduce to only two $[\vartheta(0)=\vartheta(L)=0]$ when polar angles are used. The two missing boundary conditions are recovered by further considering that also "bulk" information has been lost when passing from Cartesian components to polar ones. Indeed, consider the limit of the derivative

$$\varphi'=(n_x,n_y'-n_yn_x')/(n_x^2+n_y^2)$$

as the boundaries are approached. This limit has the indeterminate form 0/0 but, applying L'Hospital's rule, and using $n_x''$ and $n_y''$ from the *bulk* equations, it is found that $\lim_{z\to0}\varphi'=\lim_{z\to L}\varphi'=0$.

The complete set of boundary conditions is then written as

$$\begin{aligned}&\vartheta(0)=0,\quad \vartheta(L)=0\ ,\\&\varphi'(0)=0,\quad \varphi'(L)=0\ ,\\&E_R^+(0)=E_{R0}e^{-i\omega t},\quad E_R^-(L)=0\ ,\\&E_L^+(0)=E_{L0}e^{-i\omega t},\quad E_L^-(L)=0\ ,\end{aligned}\tag{22}$$

where $\mathbf{E}^+$ and $\mathbf{E}^-$ are the complex amplitudes of waves traveling in the positive and negative $z$ directions, respectively. For a circularly polarized input beam, either $E_{R0}$ or $E_{L0}$ is nil.

## III. STATIONARY REGIMES

Rather than in the complete dynamics, we are interested in the asymptotic regimes which are described by the attractors of the set of Eqs. (7), (20), and (22). To find these attractors, we may exploit the invariance of our model with respect to rotations around the $z$ axis; a rotation of an angle $\Delta\varphi$ around the $z$ axis transforms the fields as follows:

$$\begin{aligned}&Q\rightarrow Qe^{i\Delta\varphi}\ ,\\&E_R\rightarrow E_Re^{\Delta\varphi}\ ,\\&E_L\rightarrow E_Le^{-\Delta\varphi}\ .\end{aligned}\tag{23}$$

Equations (7) and (20) are not changed upon this transformation, while in the boundary conditions there is but a shift in the time origin.

Because the ensemble of all attractors has the same symmetry of the dynamical system, we must expect either single symmetric attractors or symmetric subsets. In order to search for single attractors, we apply a time-dependent uniform rotation $\Delta\varphi(t)=\Omega t$ on a stationary (except for electric-field oscillations at $\omega$) configuration of fields. A periodic time-dependent set of fields is thus obtained, which during the motion covers all the configurations which can be generated from the initial one by the transformations (23). In other words, we require that the dynamical behavior of our fields be given by

$$\begin{aligned}&\vartheta(z,t)=\vartheta(z)\ ,\\&\varphi(z,t)=\varphi(z)+\Omega t\ ,\\&E_R(z,t)=E_R(z)e^{-i\omega_R t}\ ,\\&E_L(z,t)=E_L(z)e^{-i\omega_L t}\ ,\end{aligned}\tag{24}$$

with

$$\omega_L-\omega_R=2\Omega\ .\tag{25}$$

The time-independent fields $\vartheta(z)$, $\varphi(z)$, $E_R(z)$, $E_L(z)$ must then obey the following nonlinear set of equations, $\Omega$ playing the role of the eigenvalue:

$$\begin{aligned}&E_R''+\left[\frac{\omega R}{c}\right]^2\left[\frac{\bar n^2+n_o^2}{2}E_R+\frac{\epsilon_a}{2\epsilon_\parallel}\bar n^2Q^2E_L\right]=0\ ,\\&E_L''+\left[\frac{\omega L}{c}\right]^2\left[\frac{\bar n^2+n_o^2}{2}E_L+\frac{\epsilon_a}{2\epsilon_\parallel}\bar n^2Q^{*2}E_R\right]=0\ ,\end{aligned}\tag{26}$$

$$\tau_{d,\vartheta}(\vartheta'',\vartheta',\varphi',\vartheta)+\tau_{\mathrm{em},\vartheta}(\vartheta,\varphi,E_R,E_L)=0\ ,\tag{27}$$

$$t_{d,\varphi}(\varphi'',\vartheta',\varphi',\vartheta)+\tau_{\mathrm{em},\varphi}(\vartheta,\varphi,E_R,E_L)=\Omega_{\gamma1}\sin^2\vartheta\ .\tag{28}$$

To satisfy the boundary conditions for the light fields, we may set either $\omega_R=\omega$ ($\omega$ being the input frequency) or $\omega_L=\omega$, depending on the helicity of the input wave.

The dynamics described by Eqs. (24) is a steady state if $\Omega=0$, and is a limit cycle if $\Omega\neq0$. In the latter case, as mentioned in the Introduction, a frequency shift of $2\Omega$ is added to that of the two emerging polarizations, having the opposite helicity of the input wave.

A simple steady-state solution of Eqs. (26)–(28) is given by (reflection on the glasses is neglected)

$$\begin{aligned}&\vartheta(z)=0\ ,\\&\varphi(z)=(\text{not significant})\ ,\\&E_R(z)=E_{R0}\ ,\\&E_L(z)=E_{L0}\ .\end{aligned}\tag{29}$$

This is the homogeneous undistorted state (US) which sets in when the beam intensity is below the threshold. As the intensity $I$ is increased above the threshold value [7]

$$I_{\mathrm{th}}=\frac{2\pi^2c\epsilon_\parallel K_{33}}{\epsilon_a n_o L^2}\ ,\tag{30}$$

stability is lost, and new dynamical regimes appear.

## IV. ENERGY AND ANGULAR-MOMENTUM BALANCES

From Eqs. (25)–(26), some simple considerations on conserved quantities can now be made.

For a monochromatic wave of frequency $\omega/2\pi$, the magnetic field $\mathbf{H}$ is given by

$$\mathbf{H}=-i\frac{c}{\omega}\,\mathrm{rot}\mathbf{E}\ ,\tag{31}$$

so that the cycle-averaged Poynting vector $\mathbf{S}$ is

$$\mathbf{S}=\frac{c}{8\pi}\,\mathrm{Re}(\mathbf{E}^*\times\mathbf{H})=\frac{c^2}{8\pi\omega}\,\mathrm{Im}(\mathbf{E}^*\times\mathrm{rot}\mathbf{E})\ .\tag{32}$$

Because right and left polarization waves are separately monochromatic, we can use Eq. (32) to write their respective intensities $I_R$ and $I_L$ ($z$ components of $\mathbf{S}$) as

$$\begin{aligned}&I_R=\frac{c^2}{8\pi\omega_R}\,\mathrm{Im}(E_R^*E_R')\ ,\\&I_L=\frac{c^2}{8\pi\omega_L}\,\mathrm{Im}(E_L^*E_L')\ .\end{aligned}\tag{33}$$

Moreover, by using Eqs. (26), we find

$$I_R' = \frac{\omega_R}{2}\tau_{\mathrm{em},\varphi} ,$$
$$I_L' = -\frac{\omega_L}{2}\tau_{\mathrm{em},\varphi} , \tag{34}$$

where $\tau_{\mathrm{em},\varphi}$ is the $z$ component of the electromagnetic torque $\tau_{\mathrm{em}}$, given by Eq. (17). From Eqs. (25) and (34), the following noteworthy expressions can be derived:

$$\frac{\partial}{\partial z}\left[\frac{I_L}{\omega_L}+\frac{I_R}{\omega_R}\right]=0 \quad \text{or} \quad \frac{I_L}{\omega_L}+\frac{I_R}{\omega_R}=\text{const} , \tag{35}$$

which expresses the conservation of total photon flux in the process;

$$\frac{\partial}{\partial z}(I_L+I_R)=-\Omega\tau_{\mathrm{em},\varphi} , \tag{36}$$

which expresses the equality between the energy lost by the total radiation field per unit time and volume, and the work made by the electromagnetic torque on the medium;

$$\frac{\partial}{\partial z}\left[\frac{I_L}{\omega_L}-\frac{I_R}{\omega_R}\right]=-\tau_{\mathrm{em},\varphi} , \tag{37}$$

which permits us to identify the quantity

$$M_z=\frac{I_L}{\omega_L}-\frac{I_R}{\omega_R} \tag{38}$$

as the net flux of angular momentum ($z$ component) carried by the optical field. Equations (35)–(37), although derived in the framework of a classical theory, are fully consistent with the quantum prescriptions $I_R=n_R\hbar\omega_R$, $I_L=n_L\hbar\omega_L$ relating the intensities to the photon number fluxes $n_R$, $n_L$. Equations (35) and (37) are therefore the Manley-Rowe relations of the process [16]. Notice that the Manley-Rowe relations have been obtained without making use of the slow-envelope approximation.

Using the torque balance Eq. (10), we substitute for $\tau_{\mathrm{em},\varphi}$ in Eqs. (36) and (37). Integrating the resulting equations, and using the torque expressions (15) and (19), we get the following global balances, where the elastic term has vanished:

$$I(0)-I(L)=\gamma_1\Omega^2\int_0^L \sin^2\vartheta\, dz , \tag{39}$$

$$M_z(0)-M_z(L)=\gamma_1\Omega\int_0^L \sin^2\vartheta\, dz \tag{40}$$

($I=I_R+I_L$ is the total intensity of light). Equation (39) equates the energy flux lost by the radiation field (on the left-hand side) to the total work made by viscous forces per unit time (on the right-hand side). Similarly, Eq. (40) equates the angular-momentum flux lost by the radiation field to the total viscous torque. It should be noted, however, that the exchanged energy $I(0)-I(L)$ is dissipated into heat in the medium, while the angular momentum $M_z(0)-M_z(L)$ is transferred to the velocity field, and hence finally to the walls.

## V. APPROXIMATE SOLUTION

The set of Eqs. (26)–(28) is a nonlinear problem which cannot be solved exactly. Nevertheless, with some simplifying hypothesis, an analytic solution can be found. The following assumptions are made:

(i) Splay-bend distortions are small, i.e.,

$$\vartheta^2(z)\ll 1 \quad \text{for every } z . \tag{41}$$

(ii) Twist distortions are small, i.e.,

$$|\varphi'(z)|\ll\frac{1}{L} \quad \text{for every } z . \tag{42}$$

(iii) The splay-bend distortions profile is given by the first mode of the Fourier sine expansion, i.e.,

$$\sin\vartheta(z)=|Q(z)|=A\sin\frac{\pi z}{L} , \tag{43}$$

where $A$ is a constant.

(iv) The light frequency shift is small compared to the optical frequency, i.e.,

$$2|\Omega|\ll\omega . \tag{44}$$

(v) Maxwell's equations can be solved in the slow-envelope approximation, since we neglect any reflection and suppose that

$$\frac{1}{\lambda}\gg|\vartheta'| \quad \text{and} \quad \frac{1}{\lambda}\gg|\varphi'| \tag{45}$$

(the last hypothesis obviously implies $L\gg\lambda$).

Let us first solve Eqs. (26) for the light field. In view of Eq. (44), we neglect the difference between $\omega_R$ and $\omega_L$; consequently, the beam intensity $I$ is taken as a constant throughout the sample. The only effect of the birefringence of the medium is to change the beam polarization, as described by reduced Stokes parameters

$$s_1=\frac{2\,\mathrm{Re}(E_R E_L^*)}{S_0} ,$$
$$s_2=\frac{2\,\mathrm{Im}(E_R E_L^*)}{S_0} , \tag{46}$$
$$s_3=\frac{|E_R|^2-|E_L|^2}{S_0} ,$$

where

$$S_0=|E_R|^2+|E_L|^2 . \tag{47}$$

By virtue of hypotheses (41) and (42), we expand all functions of $\vartheta$ and $\varphi'$ up to order $\vartheta^3$ and $\varphi'^2$, respectively. Cross terms such as $\vartheta^3\varphi'$, etc. are also neglected.

With these simplifications, it can be shown [17,18] that Eqs. (26) reduce, in the slow-envelope approximation, to the precession equation for Stoke's vector $\hat{\mathbf{s}}=(s_1,s_2,s_3)$ given by

$$\frac{d\hat{\mathbf{s}}}{dz}=\frac{2\pi}{\lambda}[\bar{n}(z)-n_o](\cos 2\varphi(z),\sin 2\varphi(z),0)\times\hat{\mathbf{s}} , \tag{48}$$

and that $S_0$ is related to the (constant) intensity $I$ by

$$S_0(z)=\frac{16\pi}{c[n_o+\bar{n}(z)]}I . \tag{49}$$

For circular polarization, the boundary condition for Eq.

(48) is

$$\hat{\mathbf{s}}(0)=(0,0,s_{30}) , \tag{50}$$

where $s_{30}=\pm 1$ depending on the helicity of the input light. Since the reflected wave is neglected, no condition on the optical field at the final boundary $L$ is to be imposed.

To the same order of approximation, the effective index $\bar{n}$ is given by

$$\bar{n}(z)\simeq n_o\left[1+\frac{\epsilon_a}{2\epsilon_\parallel}\sin^2\vartheta\right]\simeq n_o\left[1+\frac{\epsilon_a}{2\epsilon_\parallel}A^2\sin^2\frac{\pi z}{L}\right] . \tag{51}$$

It is expedient to define a variable $u(z)$ for the phase difference accumulated between the extraordinary and ordinary wave at depth $z$ in the sample:

$$u(z)=\frac{2\pi}{\lambda}\int_0^z[\bar{n}(z')-n_o]dz' \simeq\frac{\pi n_o\epsilon_a A^2}{2\epsilon_\parallel\lambda}\left[z-\frac{L}{2\pi}\sin\frac{2\pi z}{L}\right] . \tag{52}$$

The total phase difference $\alpha=u(L)$ at the exit face of the sample is related to the constant $A$ by

$$\alpha=u(L)\simeq\tilde{L}A^2 , \tag{53}$$

where we defined the dimensionless sample thickness

$$\tilde{L}=\frac{\pi n_o\epsilon_a}{2\epsilon_\parallel}\frac{L}{\lambda} . \tag{54}$$

Notice that, although $\alpha$ is proportional to $A^2$, it cannot be considered small, because the constant $\tilde{L}$, containing the factor $L/\lambda$, may be a very large number (typical values of $\tilde{L}$ are $\sim 100$). In actual experiments, $\alpha$ can vary over many $\pi$'s. Equation (52) can be rewritten in terms of $\alpha$ as

$$u(z)\simeq\alpha\left[\frac{z}{L}=\frac{1}{2\pi}\sin\frac{2\pi z}{L}\right] . \tag{55}$$

Let us now switch to reduced Stokes parameter vector $\hat{\xi}=(\xi_1,\xi_2,\xi_3)$ as seen in the "rotating frame" which follows the angle $\varphi(z)$; $\hat{\xi}$ is connected to $\hat{\mathbf{s}}$ by

$$\begin{aligned} s_1&=\xi_1\cos 2\varphi-\xi_2\sin 2\varphi ,\\ s_2&=\xi_1\sin 2\varphi+\xi_2\cos 2\varphi ,\\ s_3&=\xi^3 . \end{aligned} \tag{56}$$

Equation (48) then reduces to

$$\frac{d\hat{\xi}}{du}=\left[1,0,-2\frac{d\varphi}{du}\right]\times\hat{\xi} , \tag{57}$$

where $u(z)$ is given is Eq. (55). This equation can be solved by a perturbative series in powers of $d\varphi/du$. The zero-order term is found out by integrating Eq. (57) with $d\varphi/du=0$. After substituting this zero-order term back into Eq. (57), another integration gives the first-order solution:

$$\begin{aligned} \xi_1(z)&\simeq -2s_{30}\int_0^z\varphi'(z')\sin u(z')dz' ,\\ \xi_2(z)&\simeq -s_{30}\sin u(z) ,\\ \xi_3(z)&\simeq s_{30}\cos u(z) . \end{aligned} \tag{58}$$

We now can move to solve Eq. (28) for the twist distortions $\varphi'(z)$. In view of Eqs. (37) and (38), we set $\tau_{\mathrm{em},\varphi}=-M_z'$ into Eq. (28); a first integration of the resulting equation then yields

$$K_{33}(1-p_2\sin^2\vartheta)\sin^2\vartheta\varphi' =M_z(z)-M_z(0)+\Omega_{\gamma 1}\int_0^z\sin^2\vartheta(z')dz' . \tag{59}$$

The slow-envelope approximate expression for $M_z$ is

$$M_z\simeq -\frac{I}{\omega}s_3 . \tag{60}$$

Using Eqs. (43), (55), and (60), we then cast Eq. (59) in the form

$$2\alpha\sin^2\left[\frac{\pi z}{L}\right]\left[1-\alpha\frac{p_2}{\tilde{L}}\sin^2\left[\frac{\pi z}{L}\right]\right]L\varphi' =\tilde{\Omega}u(z)+\pi^2\tilde{I}[s_{30}-s_3(z)] , \tag{61}$$

where we introduced the dimensionless intensity

$$\tilde{I}=I/I_{\mathrm{th}} \tag{62}$$

and the dimensionless angular speed

$$\tilde{\Omega}=\Omega\frac{\gamma_1 L^2}{K_{33}} . \tag{63}$$

Equation (61), evaluated at $z=L$, yields the following result for $\tilde{\Omega}$:

$$\tilde{\Omega}=\pi^2\tilde{I}\frac{s_3(L)-s_{30}}{\alpha} . \tag{64}$$

If the third of Eqs. (58) for $s_3(z)$ is substituted into Eqs. (64) and (61), these become

$$\tilde{\Omega}=\pi^2 s_{30}\tilde{I}\frac{\cos(\alpha)-1}{\alpha} , \tag{65}$$

$$\varphi'(z)=\frac{\pi^2}{2L}s_{30}\tilde{I}\frac{1-\cos u(z)-(1-\cos\alpha)[u(z)/\alpha]}{\alpha\sin 2(\pi z/L)} , \tag{66}$$

where in the latter equation the small term $\varphi'\alpha/\tilde{L}$ has been neglected.

The field solutions and the eigenvalue $\Omega$ just found depend on the unknown quantity $A$, or equivalently on the total phase retardation $\alpha$; this constant is to be determined from the remaining field equation, Eq. (27). To solve this equation, we rewrite it in terms of the variable $|Q|=\sin\vartheta$, and expand up to third order, to find

$$(1-p_1|Q|^2)|Q|''+(1-p_1)|Q||Q|'^2-|Q|\varphi'^2 +\frac{\pi^2\tilde{I}}{L^2}|Q|\left[1+\xi_1-\frac{4\eta}{3}|Q|^2\right]=0 \tag{67}$$

[Eq. (49) has been also used], where

$$\eta=\frac{9\epsilon_\perp-3\epsilon_\parallel}{8\epsilon_\parallel} . \tag{68}$$

Then, following Galerkin's method [19], we substitute in Eq. (67) the first sine mode, Eq. (43), and "project" the resulting equation onto the first sine mode itself [multiplying both sides by $2\sin(\pi z/L)$ and integrating throughout the film]. The result is a transcendent equation for $\alpha$

$$\alpha\left[1-\frac{1+2p_1}{4\tilde{L}}\alpha-\tilde{I}\left[1-\frac{\eta}{\tilde{L}}\alpha\right]+\frac{\tilde{I}^2}{2}G(\alpha)\right]=0 , \tag{69}$$

where $G(\alpha)$ is the function defined as

$$G(\alpha)=2\pi^2\int_0^1\frac{\sin[\alpha v(\zeta)][1-v(\zeta)][1-\cos\alpha v(\zeta)-(1-\cos\alpha)v(\zeta)]}{\alpha\sin^2\pi\zeta}d\zeta$$
$$+\pi^2\int_0^1\left\{\frac{1-\cos[\alpha v(\zeta)]-(1-\cos\alpha)v(\zeta)}{\alpha\sin\pi\zeta}\right\}^2 d\zeta , \tag{70}$$

with

$$v(\zeta)=\zeta-\frac{1}{2\pi}\sin(2\pi\zeta) . \tag{71}$$

A trivial solution of Eq. (69) is $\alpha(\tilde{I})=0$, which corresponds to the undistorted state (US) already found in Sec. III. The nonzero solutions of Eq. (69) will depend on $\tilde{I}$, and can be found by inverting the function $\tilde{I}(\alpha)$ given by

$$\tilde{I}(\alpha)=\frac{1}{G(\alpha)}\left\{1-\frac{\eta}{\tilde{L}}\alpha-\left[1-\frac{2\eta}{L}\alpha-2G(\alpha)\left[1-\frac{1+2p_1}{4\tilde{L}}\alpha\right]\right]^{1/2}\right\} . \tag{72}$$

Of the two roots of Eq. (69) we chose the one falling in the experimental range $0<\tilde{I}<3$.

Figure 2 illustrates the typical curve $\alpha(\tilde{I})$ found from Eq. (72), for the case of a 75-$\mu$m-thick film of 4-cyano-4'-pentyl-biphenyl (5CB). The corresponding curve $\tilde{\Omega}(\tilde{I})$, as obtained from Eq. (65), is shown in Fig. 3.

For small $\alpha$, the term $\alpha/\tilde{L}$ is negligible, and the curve $\tilde{I}(\alpha)$ is well approximated by

$$\tilde{I}(\alpha)=\frac{1}{G(\alpha)}\{1-[1-2G(\alpha)]^{1/2}\} . \tag{73}$$

We note that the liquid-crystal constants $p_1$, $\eta$ and the film thickness $\tilde{L}$ have disappeared. Thus, in this approximation, the phase retardation $\alpha$ and the reduced angular velocity $\tilde{\Omega}$ turn out to be "universal" functions of the reduced intensity $\tilde{I}$, independent of the material constants, thickness, etc.

We may distinguish five regions of $\tilde{I}$, having qualitatively different features, and delimited by four critical values, $\tilde{I}_1$, 1, $\tilde{I}_2$, $\tilde{I}_3$, as shown in Figs. 2 and 3. For $\tilde{I}<\tilde{I}_1$ the only solution is the US. At $\tilde{I}=\tilde{I}_1$ there is a saddle-node bifurcation (turning point), with the appearance of two solution branches, besides US. The decreasing $\alpha(\tilde{I})$ branch (labeled RS0 in Fig. 2, for "rotating state 0") is unstable, while the increasing one (labeled "RS1") is

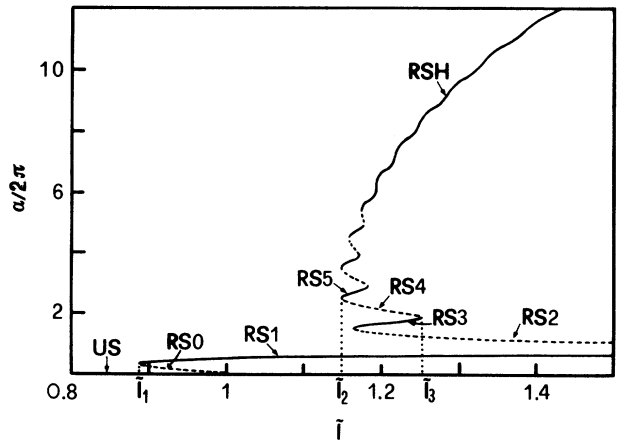


FIG. 2. Calculated total retardation angle $\alpha$ vs dimensionless intensity $\tilde{I}$ for a 75-$\mu$m film of 5CB. US, undistorted homeotropic state; RS$n$, rotating regimes (solid lines refer to stable regimes, dashed lines to unstable regimes). The critical values $\tilde{I}_1,1,\tilde{I}_2,\tilde{I}_3$ separate intensity ranges yielding qualitatively different behavior.

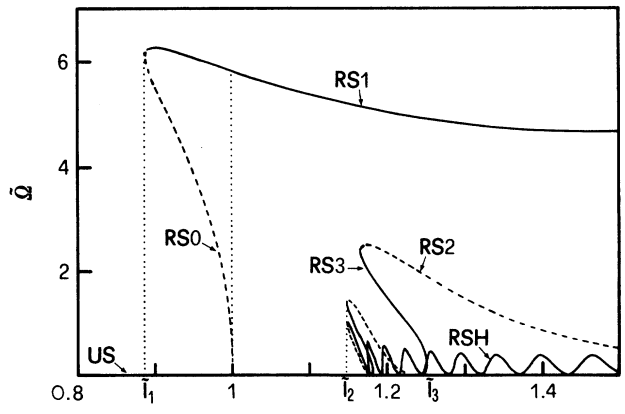


FIG. 3. Calculated dimensionless angular speed $\tilde{\Omega}$ vs reduced intensity $\tilde{I}$ for a 75-$\mu$m film of 5CB. US, undistorted homeotropic state; RS$n$, rotating regimes (solid lines refer to stable regimes, dashed lines to unstable regimes). The critical values $\tilde{I}_1,1,\tilde{I}_2,\tilde{I}_3$ separate intensity ranges yielding qualitatively different behavior.

stable. The curves $\alpha_{RS1}(\tilde{I})$ and $\tilde{\Omega}_{RS1}(\tilde{I})$ are sample independent. In this region of $\tilde{I}$ there is bistability between RS1 and US. At $\tilde{I}=1$ the system shows a Hofp subcritical bifurcation, above which US becomes unstable.

Starting from the US, and slowly increasing $\tilde{I}$, the system will remain in US up to $\tilde{I}=1$. There, it will show a first-order transition (the OFT) from US to RS1. After the transition, the system will continue to stay in the RS1 branch, even if $\tilde{I}$ is lowered below 1, showing hysteresis. Only when $\tilde{I}<\tilde{I}_1$ the system will relax back to US. The predicted value $\tilde{I}_1=I_1/I_{\rm th}\simeq 0.88$ is essentially independent of the sample.

In the range $1<\tilde{I}<\tilde{I}_2$ there are two solutions, US and RS1, but only RS1 is stable. At $\tilde{I}=\tilde{I}_2$, there is the first of many saddle-node bifurcations, which give rise to new branches of solutions alternatively stable and unstable (labeled RS2, RS3, etc.). Since the value of $\alpha$ at these bifurcations are large, the threshold $\tilde{I}_2$, as well as the number of simultaneous stable solutions depend on sample constants. All these branches disappear in subcritical bifurcations, except for the lower one (RS2) and the higher one (labeled RSH). At $\tilde{I}=\tilde{I}_3$ we are left with only four solutions, which are the US (unstable), the RS1 (stable), the RS2 (unstable), and the RSH (stable). Bistability is therefore expected, but in this case the model does not predict a threshold to go from RS1 to RSH.

We finally describe the $\tilde{\Omega}(\tilde{I})$ curve (see Fig. 3). The RS1 branch, corresponding to the less-distorted regime, and to the lowest viscous torque, has the highest velocity $\tilde{\Omega}$. Moreover, $\tilde{\Omega}$ is only slowly dependent on $\tilde{I}$ because $\alpha_{\rm RS1}(\tilde{I})$ is almost constant. On the contrary, the RSH branch has an oscillatory behavior due to the $\cos(\alpha)$ term in Eq. (65). The values of $\tilde{I}$ at which $\tilde{\Omega}_{\rm RSH}=0$ correspond to steady states with a free $\varphi$ value (the symmetric limit cycle degenerates into a symmetric ensemble of fixed points). In these states, the angular momentum transfer $M_z(0)-M_z(L)$ vanishes.

## VI. THE EXPERIMENT

We used films of 4-cyano-4'-pentyl-biphenyl (5CB) and of nematic-liquid-crystal mixture $E7$ of various thicknesses (50, 75 and 110 $\mu$m), contained between glass slides coated with surfactant for homeotropic alignment. The samples were put into an oven for temperature control within $\pm 0.1\,^{\circ}$C. The light beam was a 514.5-nm wavelength $Ar^+$ laser, focused onto the sample to a spot of about 150-$\mu$m diameter.

The experimental apparatus is shown in Fig. 4. We made an ellipsometric real-time analysis of the light beam emerging from the sample. The angular speed $\Omega$ was measured by observing the rotation of the polarization ellipse major axis. The birefringence $\alpha$ (modulo $2\pi$) could also be calculated from the output ellipticity $s_3(L)\simeq s_{30}\cos\alpha$. The number of $2\pi$'s to be added to such determination of $\alpha$ was found by counting the rings in the far-field diffraction pattern.

As a typical example, Fig. 5 shows data obtained with a 110-$\mu$m-thick $E7$ sample, together with the theoretical curve. As shown by the figure, there is a generally good agreement, especially if one considers that we used no adjustable parameters. The (RS1-US) hysteresis loop is quantitatively well reproduced by our model. On the contrary, for $\tilde{I}>\tilde{I}_2$, theory shows only a partial agreement with the observed behavior. In particular, the multistability in the $\tilde{I}_2$–$\tilde{I}_3$ range was not observed. Moreover, as shown in Fig. 5, a second hysteresis loop is found between RS1 and RSH. Although the last two regimes were predicted to be simultaneously stable, no explanation for the RS1→RSH transition is found in our model. The observed transition intensity $\tilde{I}_4$ shown in Fig. 5, however, did not show a fixed value; rather, it would change from one experiment to the other (with the same sample) by more than 20%. For comparison, the fluctuation of the observed turnoff intensity $\tilde{I}_1$ in various experiments (even with different samples) was less than 3%.

We believe that the failure of the model in the high-intensity region arises because the rotational symmetry is not completely reproduced in the experiment, due to unavoidable perturbations. The symmetry-breaking agents create a coupling of the dynamical variables $\alpha$ and $\varphi$, which, during the rotation, induces a synchronous oscil-

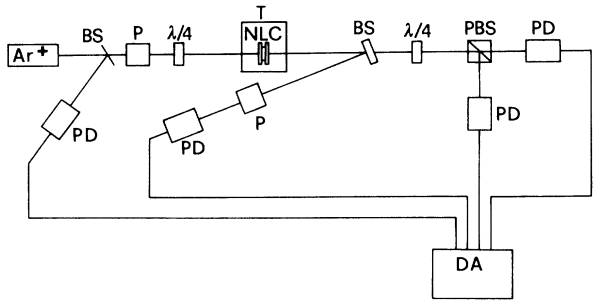


FIG. 4. Experimental apparatus. NLC, sample; $T$, thermostatic oven; $Ar^+$, laser; BS, beam splitter; $P$, polarizer; PBS, polarizing beam splitter; $\lambda/4$, birefringent plate; PD, photodiode; DA, data-acquisition system.

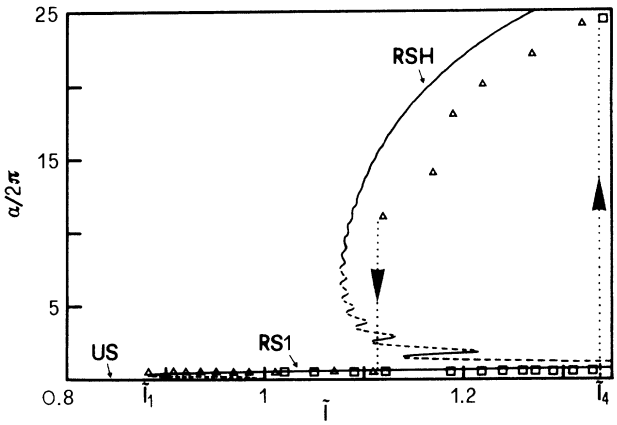


FIG. 5. Measured total retardation angle $\alpha$ vs dimensionless intensity $\tilde{I}$ for a 110-$\mu$m film of $E7$. Squares refer to data obtained with increasing intensity, triangles with decreasing intensity. Lines refer to theoretical predictions. The threshold value $\tilde{I}_4$ refers to the observed RS1→RSH transition (not explained by the model). No fitting parameters have been used.

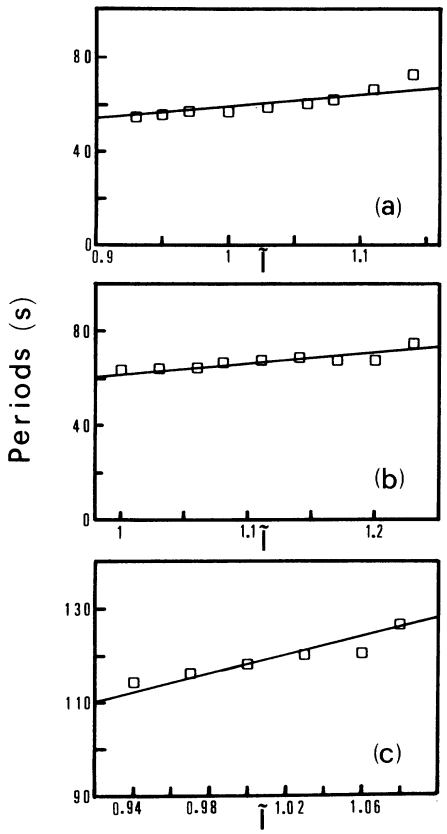


FIG. 6. Rotation periods vs reduced intensity $\tilde{I}$ in a 75-$\mu$m film of 5CB at a temperature of 24 °C [(a) and (b)], and in a 50-$\mu$m film of $E7$ at a temperature of 20 °C [(c)]. Best fits to data yielded $\tau=\gamma_1 L^2/K_{33}=55$ s in (a), $\tau=56$ s in (b), and $\tau=108$ s in (c).

lation of $\alpha$. The "nutation" was actually observed, but it remains very small for $\tilde{I}<1$, while it becomes larger and larger as $\tilde{I}$ is increased. It is probably the nutation that destabilizes the RS1 state at $\tilde{I}=\tilde{I}_4$ and that makes the RS$n$ intermediate regimes hardly observable.

In the $\tilde{I}<\tilde{I}_2$ region, the measured rotation periods agree very well with theoretical predictions, as shown in Fig. 6. The theoretical curve is given by $2\pi/\tilde{\Omega}_{\mathrm{RS1}}(\tilde{I})\tau$, where $\tilde{\Omega}_{\mathrm{RS1}}(\tilde{I})$ is the dimensionless angular speed, and $\tau$ is a time scale employed as a fitting parameter; the best fit values of $\tau$ are experimental estimates of the time constant $\gamma_1 L^2/K_{33}$ [see Eq. (63)]. The obtained values agree fairly well with reported data. For example, in the 75-$\mu$m-thick sample of 5CB, at a temperature of 24 °C, we found $\tau=55.5\pm0.5$ s, which taking $K_{33}=9.5\times10^{-7}$ dyn from Ref. [20] gives $\gamma_1=94\pm1$ cP, in excellent agreement with the value $\gamma_1=95$ cP reported in the same reference, and obtained with a completely different technique. Because our determinations of $\gamma_1$ are based on the $\varphi$ angle dynamics, and not on the $\vartheta$ angle, the measurement is not affected by backflow [13,14].

An example of application of this new measurement technique is shown in Fig. 7, where the ratio $\gamma_1/K_{33}$ in

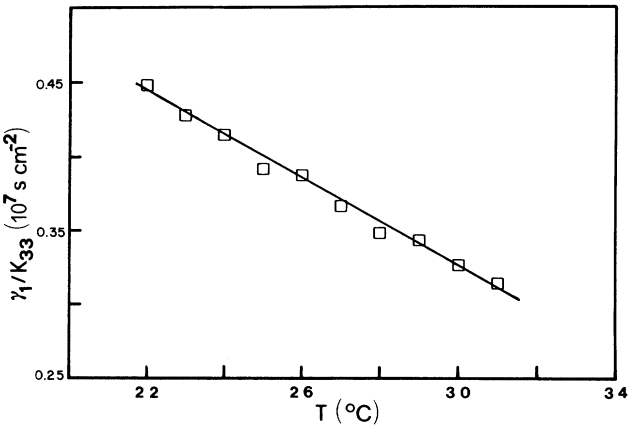


FIG. 7. Experimental values of the ratio $\gamma_1/K_{33}$ in $E7$ at different temperatures. The straight line is from linear best fit.

$E7$ is plotted as a function of temperature.

As expected, the observed RSH regime rotation is much slower than that of RS1. A quantitative fitting to the theoretical curve was nevertheless impossible in the RSH regime. The observed rotation was not even uniform, due to the simultaneous nutation.

## VII. CONCLUSIONS

We have presented a complete theoretical model for the dynamical effects induced in a NLC film by a circularly polarized laser beam, when self-induced stimulated light scattering (SISLS) takes place.

The equations for the energy and angular momentum exchange between light and matter have been derived from Maxwell's equations, in the plane-wave approximation. The Manley-Rowe relations for the process were also obtained.

With suitable approximations, which appear to be well verified in the experiments, an analytic solution to our model equations was found. In a wide range of beam-intensity values, the quantitative predictions, expressed in dimensionless variables, turn out to be independent of the material, film thickness, and light wavelength.

The comparison between theoretical results and experimental data shows excellent quantitative agreement at intensities below and slightly above the OFT threshold; only partial agreement is found when the beam intensity is increased.

Finally, by fitting the theoretical periods of rotation to the observed ones, we obtained accurate measurements of the ratio $\gamma_1/K_{33}$, free of the influence of backflow. Work is in progress, to extend and improve this technique.

## ACKNOWLEDGMENTS

This work was supported by Ministero dell'Università e della Ricerca Scientifica e Tecnologica, and by Consiglio Nazionale delle Ricerche, Italy.

[1] E. Santamato, B. Daino, M. Romagnoli, M. Settembre, and Y. R. Shen, Phys. Rev. Lett. **57**, 2423 (1986).
[2] E. Santamato, G. Abbate, P. Maddalena, L. Marrucci, and Y. R. Shen, Phys. Rev. Lett. **64**, 1377 (1990).
[3] E. Santamato, B. Daino, M. Romagnoli, M. Settembre, and Y. R. Shen, Mol. Cryst. Liq. Cryst. **143**, 89 (1987).
[4] S. D. Durbin, S. M. Arakelian, and Y. R. Shen, Phys. Rev. Lett. **47**, 1411 (1981).
[5] A. S. Zolot'ko, V. F. Kitaeva, N. Kroo, N. I. Sobolev, and L. Csilag, Pis'ma Zh. Eksp. Teor. Fiz. **32**, 170 (1980) [JETP Lett. **32**, 158 (1980)].
[6] B. Ya. Zel'ovich, N. V. Tabiryan, and Yu. S. Chilingaryan, Zh. Eksp. Teor. Fiz. **81**, 72 (1981) [Sov. Phys. JETP **54**, 32 (1981)].
[7] B. Ya. Zel'dovich and N. V. Tabiryan, Zh. Eksp. Teor. Fiz. **82**, 1126 (1982) [Sov. Phys. JETP **55**, 656 (1982)].
[8] H. L. Ong, Phys. Rev. A **28**, 2393 (1983).
[9] E. Santamato, M. Romagnoli, M. Settembre, B. Daino, and Y. R. Shen, Phys. Rev. Lett. **61**, 113 (1988).
[10] G. Abbate, P. Maddalena, L. Marrucci, L. Saetta, and E. Santamato, J. Phys. II (Paris) **1**, 543 (1991).
[11] P. G. de Gennes, *The Physics of Liquid Crystals* (Oxford University, Oxford, 1974).
[12] S. Chandrasekhar, *Liquid Crystals* (Cambridge University, London, 1977).
[13] F. Brochard, P. Pieranski, and E. Guyon, Phys. Rev. Lett. **28**, 1681 (1972).
[14] P. Pieranski, F. Brochard, and E. Guyon, J. Phys. **34**, 35 (1973).
[15] L. D. Landau and E. M. Lifshitz, *Electrodynamics of Continuous Media* (Pergamon, New York, 1959).
[16] J. M. Manley and H. E. Rowe, Proc. IRE **47**, 2115 (1959).
[17] H. Kubo and R. Nagata, J. Opt. Soc. Am. **73**, 1719 (1983).
[18] E. Santamato and Y. R. Shen, J. Opt. Soc. Am. A **4**, 356 (1987).
[19] C. A. J. Fletcher, *Computational Galerkin Methods* (Springer-Verlag, New York, 1984), Chap. 1.
[20] K. Sharp, S. T. Lagerwall, and B. Stebler, Mol. Cryst. Liq. Cryst. **60**, 215 (1980).